Assessing the Fidelity of Haptically Rendered Deformable Objects

Peter Leškovský* Matthias Harders† Gábor Székely‡

Computer Vision Laborarory
ETH Zürich
8092 Zürich, Switzerland

ABSTRACT

A central element of surgical simulators is the generation of appropriate haptic feedback. Several factors influence this rendering process, which could potentially degrade the feedback quality. In this context, our current research aims at assessing, how well haptic sensations encountered during interaction with real objects, can actually be approximated in a virtual environment. Since finding appropriate soft tissue deformation models for real time interaction is a complex task in itself, we limited the investigations in this pilot study to simple linear-elastic silicone objects.

A model of a virtual deformable object was adapted and parameters selected to approximate a real silicone sample within a specific hardware setup. A comparative study was performed, in which 13 subjects had to discriminate between the categories of real and virtual objects. We found that subjects could discern between the categories with a mean accuracy of 63% with no significant bias towards assuming the presence of either real or virtual objects. While being above chance level, the results indicate that we were able to approximate haptic feedback of a real object with high fidelity in our specific hardware setup.

Keywords: haptic rendering, haptic turing test

1 INTRODUCTION

An indispensable part in most surgical simulator systems is the display of haptic feedback while interacting with deformable tissue. Accurate rendering of organ compliance is necessary for surgeons to be able to discriminate between different tissues. A number of factors influence the quality of haptic feedback in this case - among them are the selected mechanical deformation model, material laws and setting of mechanical parameters, collision detection, tool-tissue contact handling, simulation and haptic update rates, coupling between display and simulation, and the characteristics of the haptic device used. Several points in this rendering chain exist, where errors can be introduced, simplifications have to be made, or device limitations are reached. This raises the question of how well the behavior of a real deformable object can actually be approximated with a virtual representation.

Biological soft tissue is a complex material to represent, showing characteristics such as viscoelasticity, inhomogeneity, anisotropy, or load cycle conditioning. Therefore, we started our investigations in this pilot study with the evaluation of simple, linear elastic objects. To this end, we designed an experiment, where participants were asked to compare haptic feedback during interaction with real and virtual deformable objects. The virtual model was composed of an enhanced, volume-preserving mass-spring-damper model, with parameters tuned according to measurements of real material. Haptic rendering during interaction was performed with a haptic proxy paradigm. Moreover, it should be noted, that the environment was optimized for the specific haptic interface used. The experimental task was the indentation of a soft object by a rigid tool. We compared the virtual interaction to the real poking of a silicone cylinder with a metal ball indenter.

The paper is organized as follows: after a review of related work, Section 3 introduces the virtual deformation model. Moreover, the deformation parameter setting according to a reference silicone object is described. The complete haptic system used for the experiment is presented in Section 4. In Section 5 the study performed with 13 participants is described, followed by the discussion of results and the conclusion.

2 RELATED WORK

In the past, several real-time computational models were proposed for soft tissue deformation - most of them also having been used for providing haptic feedback in simulations. First attempts defined deformation states of volumetric objects by hand-adjusted 3D force profile functions [1]. Other approaches model volumetric chainmail-like behavior of the soft matter [12]. Physically inspired mass-spring models [13] have experienced more widespread use in computer simulation. Although they lack deformation realism due to a simplified physical model, they are easily implemented and computationally effective. More accurate simulations of deformable objects can be achieved with methods stemming from mechanical engineering. Options are the boundary element method [14] or finite element method [4], however, more complex computations make real-time interaction unfeasible. While all these methods rely on meshes for topology representation, recently meshless approaches have also been proposed, e.g. based on particle systems [23], or the method of finite spheres [6].

Knowing the drawbacks of each technique (speed and correctness), these techniques were used in haptic rendering for estimating contact force, when a tool pushes on an object. These force vectors are then presented to the user via a haptic interface - usually after additional smoothing. Apart from these deformation methods, another option for getting force estimations is the exact measurement of interaction forces in the real world and their successive rendering on a device [18]. Unfortunately, the quality of the haptic feedback achieved with these approaches as compared to a reference object is only seldomly investigated.

In [15] a physical ground truth for validating the force computation of a real-time soft tissue deformation model was presented. The authors compared the deformation of the virtual model to that of a real silicone cube, the *Truth cube*. With known material properties and controlled boundary conditions, a set of volumetric displacement data was obtained. Taking this data as a ground truth, the deformations of identical situations, computed using a virtual model, can be qualitatively compared.

Several studies focusing on evaluation of haptic perception related to interaction with deformable objects were performed. These mostly examined the human haptic sensory limitations, thus pro-

*e-mail: pleskovs@vision.ee.ethz.ch
†e-mail: mharders@vision.ee.ethz.ch
‡e-mail: szekely@vision.ee.ethz.ch

viding specifications for the design of new haptic systems. Weber fractions for stiffness, force, and displacement discrimination, as well as investigations of force and compliance contrast necessary for detection were presented in [9]. Also, haptic illusions and cross-modality dependence, e.g. influence of the visual cues on the haptic perception [10], or the size and position influence of the force sensation, were examined. However, none of these studies compared the interaction with a virtual model to a real scenario.

In recent work, a research group at the Stanford University validated haptic rendering algorithms for rigid object interaction [16]. Several test subjects were asked to rate how well a virtual scenario represented the experience of tapping on a real wood sample. During the experiment a number of different rendering methods for a hard wooden surface were presented to the users. Unfortunately, the hard contact with a wooden sample could not be fully reproduced.

A comparison of haptic rendering techniques of tool-tissue contact was performed within a study on cutting of soft tissue with surgical scissors [20]. It included display of recorded data, as well as of forces obtained from a linear approximation of the empirical data. Subjects were not able to discriminate between the two approaches. The study concluded, that for modelling of cutting forces, a close approximation of real feedback might be sufficient.

3 Virtual object representation

3.1 Force computation model

With regard to the background of surgical simulation, we selected a mass-spring model approach for our experiments [2]. While simpler models could also have been used for our special test, these have only limited adaptability and can not easily be extended to general interaction with a 3D object. For instance prerecorded data can only be used within well-defined boundary conditions, which are not available in situations allowing unrestricted 3D interaction.

The dynamics of the mass-spring model is governed by Newton's second law of motion:

$$M\frac{\partial^2 x}{\partial t^2} + D\frac{\partial x}{\partial t} + F_{internal} = F_{external}\,,$$

where M is the mass matrix, D damping matrix, and F internal or external forces respectively. An explicit numerical integration of the node positions and velocities was performed. Additionally, volume preserving forces of the tetrahedral structure were imposed on each vertex. Since this choice made the virtual sample stiffer, the determined Young's modulus had to be slightly adapted to match the measured indentation force curves.

The coupling of the haptic device to the deformation simulation was done with proxy-based haptic rendering [21]. A linear spring between the proxy object and the real position of the tool tip was used for the approximation of the user's interaction force. The external force generated from the haptic proxy model was subsequently distributed to the mass-spring model nodes of the contacted surface triangle. The distribution was based on barycentric coordinates of the interaction point with respect to the vertex positions of the contacted surface triangle. Therefore, for a contact triangle ΔABC, and a contact point with coordinates $P = \alpha A + \beta B + \gamma C$ we can write:

$$F_{haptics} = \alpha F_A + \beta F_B + \gamma F_C$$

where $F_{haptics}$ is the haptic force given by the proxy model, F_A, F_B, F_C are the external forces acting on the nodes A, B, C respectively, and α, β, γ are the barycentric coordinates of the contact point with respect to a triangle ΔABC.

Two approaches for representing the proxy object were examined: a point-based paradigm, and a sphere-based interaction. The sphere-based representation was modified from the point-based model, where the force was recomputed in order to compensate for the spherical shape of the indenter tip used in our tests. According to a Herzian model of an elastic contact between a hyperspace and a spherical indenter, the indentation force depends non-linearly on the indentation depth (see also [17]):

$$F = \frac{4}{3}\sqrt{R}\,\frac{E}{1-\nu^2}\,\delta^{\frac{3}{2}}\,,$$

(where E and ν are the Young's modulus and the Poisson constant of the elastic material respectively, R is the radius of the ball indenter and δ is the indentation depth). For the sphere-based representation, a nonlinear spring $F = c.\delta^{\frac{3}{2}}$ (with a stiffness c) was used to approximate the haptic output force, while a linear spring was used to compute the external force acting on the mass-spring model. In Figure 1 the force profiles of the measured force response of the real sample and the computed forces from the mass-spring model (with proxy point and proxy sphere based rendering) are depicted. The mass-spring force profile is obtained from the inner forces acting on the middle node of the mass-spring model's top surface. This node was the nearest surface node to the contact point during the whole indentation and thus it approximates best the force profile of the internal forces acting at the contact point. These forces are then coupled to the haptic device via some of the proposed proxy models.

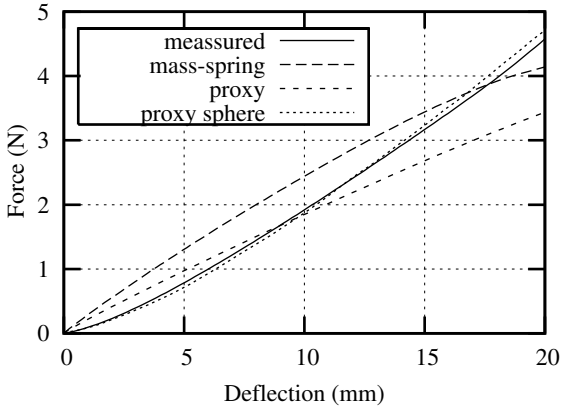

Figure 1: Force profiles of proxy-based contact force estimation.

Since the tool shape influences the magnitude of the contact force, it would be appropriate to also take the shape of the indenter tip into consideration. However, due to some instabilities encountered with the proxy sphere approach, which would have been easily recognized by a user during an experiment, we only used the point based paradigm.

3.2 Reference silicone sample

One of the main drawbacks of mass-spring models is the necessity to set deformation parameters. Spring constants, masses, and mesh topology have to be adapted to obtain a specific deformation behavior. Since manual tuning is extremely tedious, we determined the parameters from a reference silicone sample.

To obtain a material of near linear-elastic properties, we used a two part silicone rubber called ECOFLEX (Smooth-On). The mixing proportion was 3:2:1 for Ecoflex 0040 part B, silicone thinner, and Ecoflex 0030 part A, respectively. The material exhibited similar behavior to soft tissue in the linear range. We created six

cylindrical rubber phantoms for our studies. In the following discussions, the real samples are labeled ranging from R1 to R6, while the virtual models are labeled V1 to V6.

In order to determine the material properties of the assembled silicone rubber, an aspiration test has been performed as described in [19]. According to these tests, the silicone phantom could be considered as a neo-Hookean material with Young's modulus of $23.5kPa$ and assumed Poisson's ratio of 0.499. This result was also subsequently verified by a hyper-elastic FE model [24].

3.3 Parameter setting

The process of the parameter setting for one virtual object was carried out with the reference sample. For the mass-spring simulation, a mesh representation of the cylindrical object has to be created. The object has been uniformly tetrahedralized with 300 nodes, 1656 edges and 1156 tetrahedrons. Moreover, mesh parameters of the mass-spring system have to be tuned to match the assembled silicone cylinder.

The mass of the reference sample, $400g$, has been distributed to nodes of the virtual sample according to [8]. Mass moments up to the order two were matched to the moments of a cylindrical object according to

$$\int_{Body} u_x^j u_y^k u_z^l \rho(\vec{u}) d\vec{u} = \sum_{i=1}^{n} u_{xi}^j u_{yi}^k u_{zi}^l m_i \ , j+k+l \leq 2$$

where the mass of each node is m_i and its position u_i. For solving this under-determined system we applied a least-squares minimization of the distributed masses to the masses m_i of each node v_i estimated by the volume of tetrahedrons incident upon v_i:

$$\min \left(\sum_i \left(m_i - c \sum_{v_i \in T} Volume(T) \right)^2 \right) ,$$

where c is a mass correcting constant and T a tetrahedron defined by the model mesh. The determined node masses in the virtual model varied from $0.4g$ to $3.3g$.

Similar to [11], the stiffness of each spring e was set to

$$k_e = \frac{E \sum_{e \in T} Volume(T)}{Length(e)^2} ,$$

where E is the Young's modulus. Obtained spring constants varied from $0.023N/mm$ to $0.318N/mm$.

Furthermore, simulation time-step and node damping have to be set. As a starting value for the time-step we used

$$\Delta t \approx \sqrt{\frac{mass}{n \pi^2 k_{max}}} ,$$

where k_{max} is the maximum spring stiffness, n the number of nodes and $mass$ is total mass of the object (see [7]). This equation estimates the time step beyond which the system of equations of motion, using an explicit numerical integration method, is divergent. Nevertheless, since the stiffness of the springs and the mass of the nodes in our model varies, we could select a larger simulation time step. The node damping was selected manually to ensure stability of the dynamic deformation.

After setting the parameters for the mass-spring model, the constants for the virtual coupling to the proxy also have to be determined. With a stiffness value of $0.8N/mm$ we obtained stable force rendering. It has to be mentioned, that the estimated stiffness of the mass spring model, for the region where the indentation test was applied, was $0.25N/mm$. To further reduce instabilities and slight vibrations, a linear average filter was applied to smooth the position of the proxy point between successive updates of the mass spring model:

$$\tilde{n} = \frac{t_{haptics}}{2t_{simulation}} , \tilde{F} = \frac{F_{t-\tilde{n}} + \ldots + F_t}{\tilde{n}} .$$

The size of this filter was set to half of the ratio between the haptic and virtual object update rates. Using this approach the step-like response of the proxy force was reduced.

4 System setup

For our experiments we chose the PHANToM Premium Model 1.5 (by SensAble Technologies, Cambridge, MA) to provide the interface for indenting the real and virtual samples. The selection of the device was dominated by availability. Considering the limitations of the device's force response [5][3], we do not claim, that the device was optimal for our task. One significant problem we experienced has been due to the limited maximum forces of the device. From empirical tests, this was estimated to be around $4N$. It has to be remembered that due to the parasitic inertia and friction of the selected hardware (in the haptic device, as well as in the overall construction described later in Section 5.3), the results are only valid in this specific setting.

The test application has been run on a Linux PC with 2xP4 2.8GHz processors. We used two asynchronous threads: one for haptic force rendering using the proxy model and one for deformation calculation. During the experiments the haptic thread was running at 1kHz, while the deformation calculation was running with an approximate refresh rate of 100Hz.

5 Discrimination experiment

5.1 Overview

In order to evaluate the quality of the haptic rendering, we carried out a discrimination experiment related to indentation of real and virtual objects. Participants were asked to push with a metal ball indenter onto a real silicone cylinder, or on the virtual object respectively. The whole task was performed blindly. After several indentations, users were asked whether they believed to have touched a real or virtual object. Because free tool-object interaction would involve many contact effects (e.g. friction, multiple contact points, torques, etc.), which would influence the interaction, the whole procedure was limited to one-dimensional interaction. Touching the body was possible just in one point (the middle of the object's top surface), and only in vertical direction. The forces rendered on the haptic device have also been restricted to this direction. However, contact forces and the inner forces of the virtual object, governed by the mass-spring model, were still computed in all directions for the whole body. For this initial study, interaction was limited to slow movements only (the average contact speed was about $0.1m/s$). This can partly be justified with regard to our application area of surgical simulation, where surgeons usually interact in a controlled, steady manner.

5.2 Participants

Thirteen participants (two female, eleven male), took part in the test. Their age ranged from 26 to 54 years (with an average of 30 years). All but two subjects were right-handed (although just one was using the left hand for the tests). None of them reported any known haptic deficit due to an accident or illness. Two participants were experienced PHANToM users. While most of the others users already experienced haptic simulations with the PHANToM before, they can not be considered as experienced users of haptic devices.

5.3 Experimental apparatus

The experiment was performed with a PHANToM haptic device as previously described. A 250*mm* long pen-shaped stylus was attached at one end to the robot arm of the PHANToM device. On the other end of the pen a ball intender was fastened. In order to find a trade-off between substantial penetration depths and pure elastic deformation of the real samples, we used a ball indenter with a radius of 4*mm*. This allowed indentation depths of up to 20*mm* while still being able to reproduce the same behavior with the PHANToM device. The stylus was sliding inside a 30*mm* long tube, equipped with ball bearings to ensure resistance free motion. This limited the interaction to one direction. To avoid side vibrations coming from the rigid side-grip of the stylus inside the tube, the computed PHANToM forces have been projected to the same direction. Beneath the indenter, six real samples were placed on a rotatable support while leaving place for virtual samples. A blocking system of the rotatable plate allowed for fast and precise positioning of the middle of each sample below the indenter. The whole setup was put behind a tall barrier to prevent the user from observing the apparatus during the test. A complete view of the test setup can be seen in Figure 2.

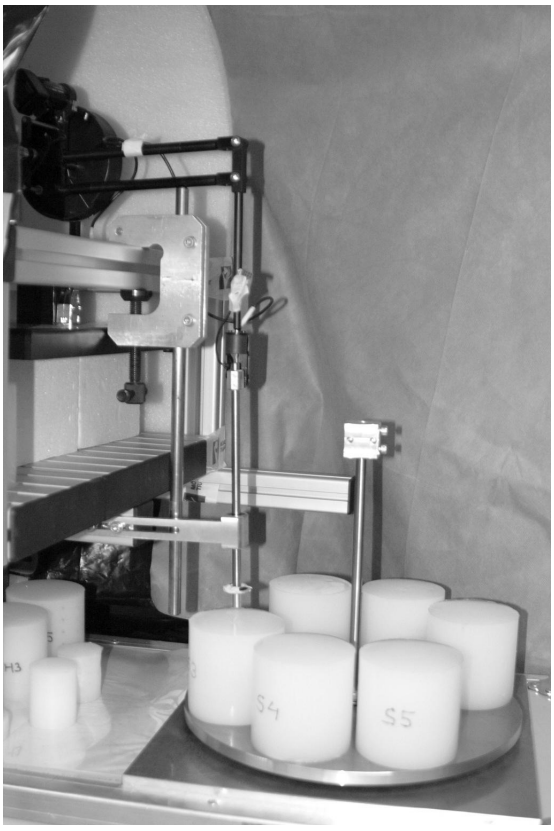

Figure 2: Experimental setup with a PHANToM, attached indenter driven in a tube, and a rotatable sample support.

Participants sat at a table and put their hand through an opening in the barrier. Through the opening the users were holding the pen-shaped indenter. During the whole test the participants could rest their arm on a support. In the setup the user could freely move the indenter up and down for 40*mm*, without getting into contact with the surrounding construction. The indentation depth was limited to approximately 20*mm* by a rigid stop, due to the mentioned force rendering limitations of the PHANToM device. To mask the sound of the PHANToM motors and the ball bearing, users wore closed headphones as acoustic ear protectors with white noise played. No additional visual feedback, e.g. from the virtual simulation, was provided to the user, thus each participant had to make his decision just according to the haptic stimuli he received. The operator was on the other side of the barrier monitoring the progress and changing the samples beneath the indenter.

5.4 Procedure

The experiment consisted of two phases: training session, and testing. The objective of the training phase was two-fold. Firstly, a user should get used to the setup and the haptic feedback in general. This included the limits of the desired interaction style. Participants were instructed to slowly approach the objects with the indenter, always hold the indenter in their hand during the interaction, perform just slow movements (approximately two punches per second) and move within the non-restricted range of 20*mm* indentation depth (before hitting the rigid stop).

Secondly, the two categories of real and virtual objects were presented, so that the user can determine the differences between both classes. To this end, he could experience the interaction between one real sample and a virtual one, whose elastic properties have been tuned to match the real object as described in Section 3.3. This phase lasted till the participants felt comfortable with the apparatus and were ready for the main test.

During the testing phase, subjects were told that they will be presented several real objects with small differences in stiffness and height. Additionally, virtual objects, with similar deformation characteristics to the real objects, will also be shown among the real samples. The user was informed, that her task is to express her estimate if interacting with a real or a virtual object.

For each subject the test consisted of 50 trials, where a randomly selected object from the six real and six virtual models was presented to the user within each trial. No response feedback was given to the participants after each trial.

5.5 Conditions

Between all real samples there were slight differences in their stiffness and their height. The stiffness variation was 35%, while the maximum difference in the sample height was 3*mm*. Additionally, six virtual cylinders were set up for the test, taking into account the parameter settings described in Section 3.3. In the following, the reference sample from the Section 3.3 and the corresponding tuned virtual sample are denoted R2 and V3 respectively. To resemble the difference in the real objects, five variations of the tuned virtual model V3 were created. They were adjusted to cover the range of heights and stiffnesses of the real samples. An overview of all objects is given in Table 1.

The different force responses of the real and virtual samples were measured and are presented in Figure 3. These measurements were made only approximately using the PHANToM device. All forces were determined from the position, where the gravity of the indenter was counterbalanced by the deformation force of the current sample, and thus at zero force response little deflection can be noticed. These measurements are not very precise and thus just the differences of the slopes of each curve should be compared.

6 Results

All participants went through the learning phase within five minutes, and completed the experiment of 50 trials on average in 20 minutes. Four different combinations of trial condition and response were possible. *Hits* occurred, when a real sample was correctly identified, and *false alarms*, when a virtual object was as-

Table 1: Estimated elasticity (Young's modulus in *kPa*) and heights (in *mm*) of the samples, real and virtual, used during the experiment. The indicated ratio is the elasticity ratio computed in reference to the object R2 and V3 for the real samples and virtual samples, respectively.

Real	R1	R2	R3	R4	R5	R6
elasticity	20.6	23.5	27	28.6	29	35.6
height	80	81.5	82.5	81	79.5	80.5
ratio	1.14	1	0.87	0.82	0.81	0.66
Virtual	V1	V2	V3	V4	V5	V6
elasticity	14.5	17	17	20.4	21.2	25.5
height	82	80	82	80	81.5	78.5
ratio	1.17	1	1	0.83	0.80	0.66

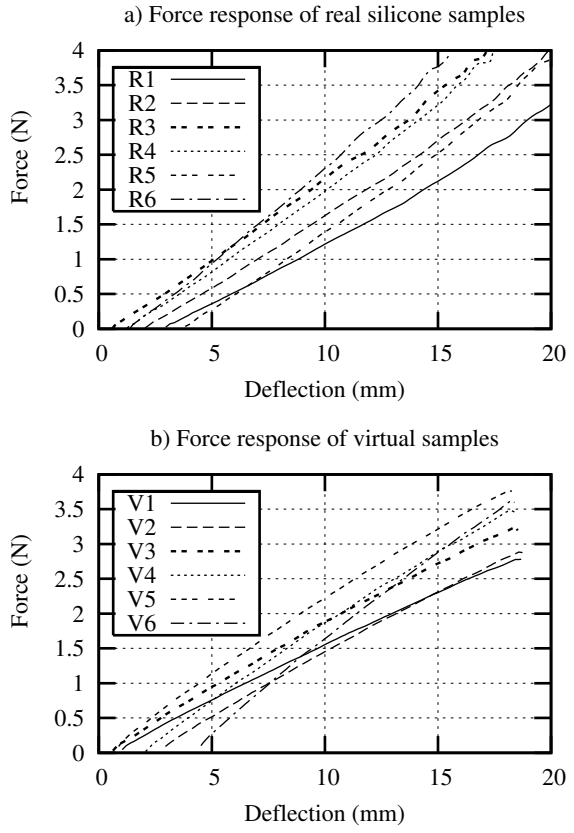

Figure 3: The recorded forces of the real and virtual samples: a) real samples, b) virtual samples.

sumed to be real. Similarly, a *correct rejection* was counted, when a virtual object was recognized as such, and a *miss* was recorded, when a real object was attributed as virtual.

Counting false alarms and misses, the mean number of wrong responses of all participants was 18.66 in 50 trials, with a standard deviation of 7.15. To further analyze the data (see for instance [22]), we start with determining hit rate H and false alarm rate F. The former describes the probability of a correct detection, when a real object was present, while the latter denotes the probability of assuming a real object, when a virtual sample was shown. In the optimal case, hit rate is high and false alarm rate low, while values around 50% indicate decision making by chance. Figure 4 a) depicts the results of our study. The mean values of hit and false alarm rate are 62.8% and 36.3%, respectively.

Two further measures have to be determined to analyze the data - sensitivity (also referred to as discriminability) and response bias. The former denotes the ability to detect the actual category of real or virtual objects, and the latter a possible tendency towards reporting a specific category more often.

As described in [22], we determine the non-parametric measure of sensitivity A' according to

$$A' = \begin{cases} 0.5 + \dfrac{(H-F)(1.0+H-F)}{4.0H(1.0-F)} & if \quad H \geq F \\ 0.5 + \dfrac{(F-H)(1.0+F-H)}{4.0F(1.0-H)} & if \quad H < F \end{cases}.$$

The measure usually ranges from 0.5, which indicates chance performance, to 1.0, which corresponds to perfect category detection. Values less than 0.5 may arise due to response confusion. The non-parametric measure of bias B''_D can be determined by

$$B''_D = \frac{(1.0-H)(1.0-F)-HF}{(1.0-H)(1.0-F)+HF}.$$

Positive values represent a tendency to report interaction with the virtual object category, while negative values represent a tendency to report the real one. Non-existent bias is indicated by values close to 0.0. Both measures are shown in Figure 4 b). Mean sensitivity is 0.707 with a mean bias of 0.01.

While we are still above chance level, the results show, that participants were unable to perfectly discriminate between the two categories. This is also reflected by comments gathered from the participants, who regarded correct discrimination of the categories as rather difficult.

To further analyze our results, we investigated whether a specific sample could be easier recognized than the others. However, no indication of this could be noticed. The mean of wrong recognition of real samples was 37.3%, with a standard deviation of 5.15%; and the one of virtual samples 36.1%, with a standard deviation of 4.74%.

We also examined, if a change in performance could be noticed during the course of the experiment. Only in two cases, the ability to differentiate between virtual and real objects improved slightly in the second half of the test. Nevertheless, this has not been statistically significant.

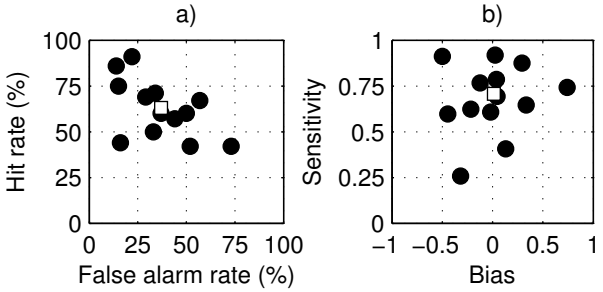

Figure 4: Statistical plots of all participants: a) Hit versus False alarm rate, b) Sensitivity versus Bias. The mean values are marked with a square.

For a further analysis, we recorded the mass-spring model generated forces and the positions, and the velocities of the indenter tip at 1kHz (see Figure 5). Due to technical limitations, we could not record the force response of the real model during the indentation test. However, an inspection of the smoothness of the force response, and a comparison of the recorded positions and velocities, for the interaction with the virtual as well as the real samples, did not reveal a clear difference of the two models.

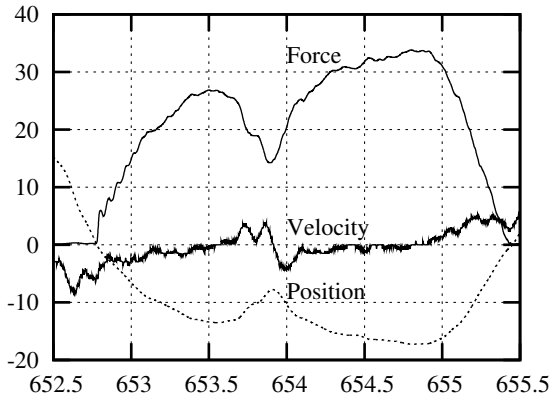

Figure 5: An example of recorded positions (scaled to mm), velocities (scaled to $10mm/s$) and forces (scaled to $10^{-1}N$) during an interaction with virtual object, which was detected correctly.

Apart from the quantitative data, after the trials we also collected comments from participants to determine their approach during the test. We found that the best detection performance was achieved by participants who reported a small difference during the first contact of the probe with the sample. It was described as a "sinking of the tool" effect. We attribute this phenomenon to the selected proxy-point simplification of the haptic rendering (see Section 3). However, all users reported the discrimination task to be very hard for deeper penetrations.

Other cues, which were sometimes present, were small vibrations encountered during interaction with the virtual model. This was due to the alignment of the indenter with the ball bearing. A small rippling effect could be noticed, which became more evident with the tilting of the moving indenter. Rendered forces could lead to such a tilt, since the direction was not perfectly aligned with the driving tube.

Moreover, two subjects reported that a low frequency wave was noticeable for a moment after stopping the indenter inside the sample, especially for the harder objects. This effect could also be verified by their data, since they performed slightly better with harder samples. The nature of this wave comes from the limited information propagation speed of the explicit numerical integration scheme used. Additionally, this effect becomes more visible for the harder objects since the parameter setting of the virtual models was not done particularly for each one.

Finally, none of our participants actually reported the haptic rendering during interaction as unrealistic or artificial.

7 Conclusions

In this study we examined the fidelity of a simple deformation model for providing haptic feedback during interaction with virtual elastic objects. Deformation parameters were determined based on reference silicone samples. A discrimination task was carried out, in which participants had to differentiate between real and virtual objects. Results showed that this task was quite complex, since only small differences between real and virtual haptic feedback could be noticed. Thus, we were able to achieve a high fidelity of virtual rendering.

While the selected tissue model was too simple to be used in surgical simulation, the experiment already indicates that a reasonable approximation of real behavior can be reached. In this respect, one also has to consider, that the participants in our study were explicitly told to look for small differences. During surgical simulation, slight deviations from perfect feedback might be acceptable, since the trainee does not fully focus on small discrepancies. Since the main target of surgical simulation should be to achieve a training effect, if, and to what degree a small deviation from real feedback would affect this process still remains an open question. However, a final answer to this problem is beyond the scope of this paper. It should also be noted, that we do not suggest to use simple deformation models for a surgical training system. The study only determined, how well forces coming from a real object can actually be approximated. Tests with more complex deformation models should also be carried.

Finally, we can also infer, that our approach for parameter tuning of our deformable models is at least sufficient to provide reasonably realistic haptic feedback. Nevertheless, an extrapolation to complex objects may not be straightforward.

In future work, several shortcomings of our system will be addressed. For the hardware setup, a better solution will be found for guiding the indenter to avoid high-frequency noise. Moreover, we will examine proxy-sphere based haptic rendering to improve the first phase of tool-tissue contact. Furthermore, since the user was limited to slow movements, the dynamics of the deformation model did not play a major role. In order to allow more free interaction with the virtual samples, the dynamics of our simulation need improvement. Finally, evaluations with more rigorous data analysis methods will also be performed.

Acknowledgements

The authors would like to thank Davide Valtorta and Alessandro Nava for processing the material parameter estimation tests of the real silicone samples. This research was supported by the TOUCH-HapSys project EU CEC IST-2001-38040.

References

[1] C. Baur, D. Guzzoni, and O. Georg. A virtual reality and force feedback based endoscopic surgery simulator. In *MMVR Art, Science, Technology : Healthcare Revolution*, pages 110–116, San Diego, January 1998. IOS Press.

[2] David Bourguignon and Marie-Paule Cani. Controlling anisotropy in mass-spring systems. In *Proceedings of the 11th Eurographics Workshop*, pages 113–123, Interlaken, Switzerland, August 2000.

[3] Gianni Campion and Vincent Hayward. Fundamental limits in the rendering of virtual haptic textures. In *WHC*, pages 263–270. IEEE Computer Society, 2005.

[4] Murat Cenk Cavusoglu. *Telesurgery and Surgical Simulation: Design, Modeling, and Evaluation of Haptic Interfaces to Real and Virtual Surgical Environments*. Phd thesis, University of California at Berkeley, Fall 2000.

[5] Murat Cenk Cavusoglu, David Feygin, and Frank Tendick. A critical study of the mechanical and electrical properties of the phantom haptic interface and improvements for high performance control. *Presence*, 11(6):555–568, 2002.

[6] S. De, J. Kim, and M.A. Srinivasan. Virtual surgery simulation using a collocation-based method of finite spheres. In *First MIT Conference on Computational Fluid and Solid Mechanics*, pages 140–141. Elsevier Science, 2001.

[7] H. Delingette. Towards realistic soft tissue modeling in medical simulation. In *Proceedings of the IEEE : Special Issue on Surgery Simulation*, pages 512–523, April 1998.

[8] O. Deussen, L. Kobbelt, and P. Tücke. Using simulated annealing to obtain good nodal approximations of deformable bodies. In *Sixth Eurographics Workshop on Simulation and Animation*. Springer, September 1995.

[9] N. Dhruv and F. Tendick. Frequency dependence of complience contrast detection. In *ASME - Dynamic Systems and Control Division*, volume 2, pages 1087–1093, 2000.

[10] L. Dominjon, A. Lcuyer, J.M. Burkhardt, P. Richard, and S. Richir. Influence of control/display ratio on the perception of mass of manipulated objects in virtual environments. In *Proceedings of IEEE International Conference on Virtual Reality*, Bonn, Germany, 2005.

[11] Allen Van Gelder. Approximate simulation of elastic membranes by triangulated spring meshes. *Journal of Graphics Tools*, 3(2):21–42, 1998.

[12] Sarah Gibson, Joseph Samosky, Andrew Mor, Christina Fyock, Eric Grimson, Takeo Kanade, Ron Kikinis, Hugh Lauer, Neil McKenzie, Shin Nakajima, Hide Ohkami, Randy Osborne, and Akira Sawada. Simulating arthroscopic knee surgery using volumetric object representations, real-time volume rendering and haptic feedback. Technical report, MERL - Mitsubishi Electric Research Laboratories, 1996.

[13] Sarah F. Gibson and Brian Mirtich. A survey of deformable modeling in computer graphics. Technical report, MERL - Mitsubishi Electric Research Laboratories, 1997.

[14] D. James and D. Pai. Artdefo: Accurate real time deformable objects. In *Computer Graphics (SIGGRAPH 99 Proceedings)*, pages 65–72, August 1999.

[15] A. E. Kerdok, S. M. Cotin, M. P. Ottensmeyer, A. M. Galea, R. D. Howe, and S. L. Dawson. Truth cube: Establishing physical standards for real time soft tissue simulation. In *Medical Image Analysis*, volume 7, pages 283–291. Elsevier, 2003.

[16] Katherine J. Kuchenbecker, Jonathan Fiene, and Gnter Niemeyer. Event-based haptics and acceleration matching: Portraying and assessing the realism of contact. In *World Haptics Conference*, Pisa, IT, March 2005.

[17] M. Mahvash, V. Hayward, and J. Lloyd. Haptic rendering of tool contact. In *Proc. Eurohaptics 2002*, pages 110–115, 2002.

[18] Mohsen Mahvash and Vincent Hayward. High-fidelity haptic synthesis of contact with deformable bodies. *IEEE Computer Graphics and Applications*, 24(2):48–55, 2004.

[19] A. Nava, E. Mazza, F. Kleinermann, N. J. Avis, and J. McClure. Determination of the mechanical properties of soft human tissues through aspiration experiments. In *MICCAI 2003*, volume 2878 of *Lecture Notes in Computer Science*, pages 222–229, 2003.

[20] Allison M. Okamura, Robert J. Webster, Jason T. Nolin, K. W. Johnson, and H. Jafry. The haptic scissors: cutting in virtual environments. In *IEEE International Conference on Robotics and Automation*, pages 828–833, Taipei, Taiwan, September 2003.

[21] Diego C. Ruspini, Krasimir Kolarov, and Oussama Khatib. The haptic display of complex graphical environments. In *Computer Graphics (SIGGRAPH 97 Conference Proceedings)*, pages 345–352. ACM SIGGRAPH, 1997.

[22] Harold Stanislaw and Natasha Todorov. Calculation of signal detection theory measures. *Behavior Research Methods, Instruments, & Computers*, 1:137–149, 1999.

[23] N. Suzuki and S. Suzuki. Surgery simulation system with haptic sensation and modeling of elastic organ that reflect the patients' anatomy. In *Proceedings of IS4TM Conference 2003*, volume 2673, pages 155–164. Springer-Verlag Heidelberg, 2003.

[24] O. H. Yeoh. Some forms of the strain energy function for rubber. In *Rubber Chemistry and Technology*, volume 66, pages 754–771, 1993.